Research Article | Vol. 27, No. 24 / 25 November 2019 / Optics Express 35621
Optics EXPRESS

3D printed stacked diffractive microlenses

SIMON THIELE,[1,*] CHRISTOF PRUSS,[1] ALOIS M. HERKOMMER,[1] AND HARALD GIESSEN[2]

[1] *Institute of Applied Optics (ITO) and Research Center SCoPE, University of Stuttgart, Pfaffenwaldring 9, 70569 Stuttgart, Germany*
[2] *4th Physics Institute and Research Center SCoPE, University of Stuttgart, Pfaffenwaldring 57, 70569 Stuttgart, Germany*
[*] *thiele@ito.uni-stuttgart.de*

Abstract: Planar lenses such as metalenses and diffractive lenses exhibit severe field-dependent aberrations when imaging extended objects with high numerical aperture. This problem can be overcome by stacking at least two of such devices on top of each other. In this work, we present such stacked imaging systems, namely doublets and triplets of diffractive optical elements. They are fabricated by femtosecond direct laser writing in one single step without the need for alignment in sizes of below 200 µm in diameter and 100 µm in height. The lenses allow for efficient sub µm resolution imaging at visible wavelengths combined with a full field-of-view of up to 60°. As additional benefit, our approach dramatically reduces the writing times of 3D printed lens systems to below 15 minutes.

1. Introduction

3D printed optical elements have recently enabled an entirely new class of complex micro-optics. Optical singlet, doublet, or even triplet refractive lenses on optical fibers [1–4], optical phase plates [5–8], beam shapers [9,10], and optical metamaterials [11] have brought unprecedented design and manufacturing flexibility into the size range below 500 µm. One drawback, so far, has been the long fabrication time for such elements, which easily could take as long as many hours. Additionally, the optical performance and functionality is somewhat limited, as a refractive surface with a given refractive index yields only refraction within Snell's law and within a certain volume element. Thus, high-NA optics demand larger elements and volumes, even on the micro-optical scale. Diffractive optical elements give us the power to overcome both issues. As they can be manufactured as thin as membranes, only a minute amount of optical material is necessary to achieve the designed function, thus printing times can be dramatically reduced. Furthermore, as they utilize diffraction, large beam deflection angles are possible within a very small printing volume. In combination with femtosecond 3D printing, this opens up the possibility for high-performance, flexible, and extremely lightweight optical elements that give nevertheless submicron imaging resolution over a large field of view, which is essential for microscopy, or miniature imaging sensors, such as in endoscopes or drones.

Here, we present 3D printed stacked diffractive imaging systems which combine the aforementioned advantages with nearly aberration-free (aplanatic) imaging for a given wavelength, allowing for high resolution imaging over an extended field of view. Our stacked diffractive optical elements can be realized with a simple one-step fabrication process and a high miniaturization of the overall device.

Flat diffractive lenses were first conceived by Augustin-Jean Fresnel [12] and then evolved into elaborate schemes [13–16] that culminated in wafer level optics [17,18] as well as in metalenses [19–24].

If flat lenses are used for imaging, strong color and coma aberrations lead to a significant decrease in image quality [25]. Field dependent monochromatic aberrations such as astigmatism,

#375689 https://doi.org/10.1364/OE.27.035621
Journal © 2019 Received 16 Aug 2019; revised 5 Oct 2019; accepted 8 Oct 2019; published 20 Nov 2019

Optics EXPRESS

coma, and field curvature can be corrected by bending a diffractive lens [26–28] or by combining multiple elements as was suggested theoretically by Bobrov [29] and later by Buralli [30]. Arbabi et al. presented a miniature metasurface camera consisting of two separated flat lenses which shows corrected imaging performance over a field of view of 70° in the near infrared [31]. Later, Groever et al. presented a similar metalens working in the visible regime [32].

A single surface can act as a perfect lens with focal length f for focusing on the optical axis if it adds a spherical phase of $\varphi(r) = -(2\pi/\lambda)\sqrt{r^2+f^2}$ to an incident wave front. However, if light is impinging under a certain angle α, the lens will not form a perfect focus unless an angle-dependent phase term $\varphi(\alpha)$ is added to the lens phase which at the same time deteriorates the performance for angles other than α. Thus, a single flat phase element cannot provide aberration-free imaging over an extended field of view. A possible solution is the combination of two or more flat lenses, inspired by the combination of two or more lenses for monochromatic aberration correction of 1st (defocusing, distortion) and 3rd (spherical aberration, astigmatism, coma, Petzval field curvature, distortion) order in multi-element lens systems. In this case, the additional degrees of freedom introduced by the distance between first and second element leads to a total phase shift which is a function of both, the pupil radius as well as the angle of incidence. In Fig. 1 both cases are compared.

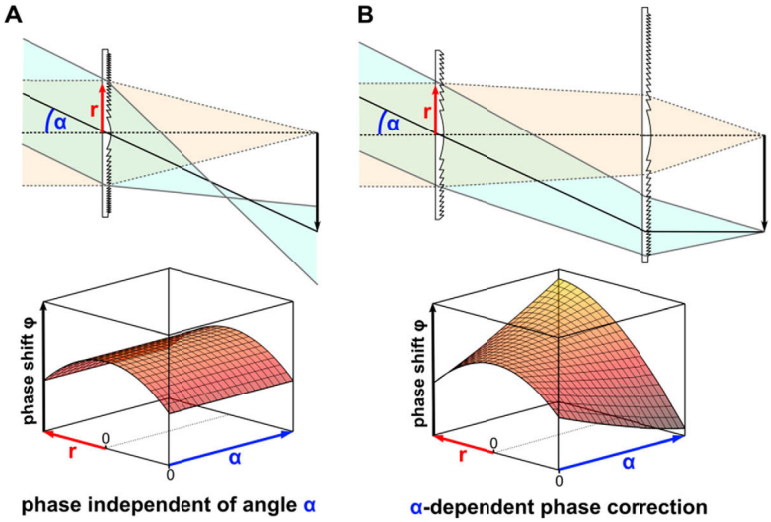

Fig. 1. Phase shift as a function of entrance pupil radius r and angle of incidence α. (A) One flat lens leads to a phase shift φ(r) but does not allow for an angle dependent control of the phase φ(r,α). This leads to strong aberrations for fields with oblique incidence. (B) If two or more lenses are combined, the phase shift φ(r, α) can be chosen as a function of both variables and thus allows an aberration-free system over a wide field of view.

2. Design and experiment

To measure diffraction efficiencies, gratings with periods from 6.3 µm to 0.67 µm (5° to 55° deflection angle at $\lambda = 550$ nm) were designed and fabricated for use in the first diffraction order. Fabrication by 2-photon direct laser writing was performed in the same way as for the lenses described in the following paragraph. The angle dependent efficiency was then determined using a collimated laser diode and a vertical microscope. Far-field diffraction patterns were obtained by imaging the Fourier plane of the microscope lens onto a CMOS chip where the different diffraction orders appear as small spots. Diffraction efficiencies were calculated by dividing the

Optics EXPRESS

integrated intensity of the 1st diffraction order through the integrated intensity passing through a flat plate with the same size and fabrication process as the gratings.

Compared to the gratings used for efficiency measurements, the imaging lens phase reliefs were designed and optimized for a different light source (slightly different wavelength: 543 nm) with the raytracing software ZEMAX (version 13) using a global optimization algorithm. The optimum phase φ as a function of radius r was determined in terms of coefficients a_i as $\varphi(r) = \sum_{i=1}^{N} a_i r^{2i}$ by using raytracing based on the local grating approximation (LGA). The total number of sum terms N was increased stepwise for each design until improvements to the merit function were negligible (singlet: N = 7, doublet: N = 12, triplet: N = 10). The necessary surface profile to create this phase in air can be calculated by modulating the phase function in steps of 2π and multiplying the result with $\lambda/(2\pi(n-1))$. The refractive index n of the material (photoresist) was measured to be 1.548 at a wavelength λ of 546.9 nm which is sufficiently close to our design wavelength of 543 nm [33]. A minimum local grating period of ~0.7 µm resulted in the outermost zones of the singlet lens which roughly corresponds to the cutoff period at which the diffraction efficiency drops significantly for visible wavelengths [34]. The final geometry of the lens stacks was optimized to reduce the amount of printed resist volume and at the same time to minimize writing times. Therefore, the diffractive surfaces were placed on thin disks (t = 8 µm) which are mounted on pillars with a wall thickness of 10 µm. All lenses were restricted to a maximum diameter of 200 µm. The designs were 3D-printed in dip-in configuration with a Nanoscribe 'Photonic Professional GT' device using IP-DIP photoresist and a 63x, NA 1.4 objective lens. As substrates, 170 µm thick borosilicate crown glass (BK7) slides with a thin layer of indium tin oxide were used. Further details about the process can be found in [4]. Typical writing times of lens systems such as the doublet lens were in the range of 15 minutes but can be further reduced. A zone-boundary optimization was performed in a way similar to [35]. AFM surface measurements were taken with a Veeco Dimension 3100 Nanoman and a high resolution tip.

The imaging performance of the devices was tested in two different configurations. In the first case, the lenses were used similar to a camera lens. The object, a USAF 1951 test target with varying line widths and spacings, was placed well beyond the hyperfocal distance of the lenses (~30 mm). The created image was then observed with an upright microscope (Nikon Eclipse LV100-DA) using aberration-corrected objective lenses (Nikon CFI LU Plan BD ELWD 50x, 0.55 NA and 100x, 0.8 NA) and a high quality camera (Nikon DS-Ri2). In the second configuration, the sample orientation was reversed and a high resolution USAF-target was placed very close to the diffractive lens focal plane. The resulting distant image could then be observed with the microscope. All measurements were carried out with the microscope white light source (Nikon LV-HL50W). In some cases a bandpass filter (Thorlabs FB550-40) with central wavelength of 550 nm and a full width at half maximum (FWHM) bandwidth of 40 nm was inserted into the beam path between microscope objective and tube lens.

Sagittal line-spread function (LSF) and modulation transfer function (MTF) curves were recorded by imaging a knife edge under Lambertian illumination with bandpass filtered light of $\lambda = 550 \pm 20$ nm. The radial distance from the optical axis was determined by analyzing resulting images and used to calculate angles of incidence based on the raytracing models. Resulting knife edge images were converted from RGB to 16 bit grey scale using the software ImageJ. Results were used to calculate the edge spread function at different positions along the knife edge by averaging over 10-40 pixels (~1.45-5.8 µm) along the edge. This edge spread function was then numerically differentiated to compute the LSF. The MTF was calculated by taking the absolute value of the discrete Fourier transform of the LSF. The MTF curves were then normalized to their maximum value. FWHM values of the LSF were obtained by fitting the measured values with a sinc^2 function and determining its full width at half maximum.

Optics EXPRESS

3. Results

The diffraction efficiency of surface-relief diffractive lenses usually drops at high deflection angles since small period to wavelength ratios, according to electromagnetic theory, lead to limitations even in case of perfectly fabricated structures [36]. A quantitative estimation of these effects was obtained by investigating the diffraction efficiency of 3D-printed blazed (triangular unit cell) linear gratings with different periods and thus different diffraction angles. These blazed gratings can be considered to locally approximate our lenses whose period decreases with increasing aperture radius. We refer to section 2 for more information about this experiment. Figure 2 shows the measured diffraction efficiency as a function of deflection angle. As expected, a reduction occurs for higher angles. At an angle of 55° which corresponds to the marginal ray angle when focusing with a numerical aperture of 0.82, a mean efficiency of 25.6% was measured. When applied to a diffractive kinoform lens, this resulting apodization decreases the effective NA. Nonetheless, high deflection angles can help to increase imaging performance as long as unwanted stray light is absorbed or scattered to uncritical directions.

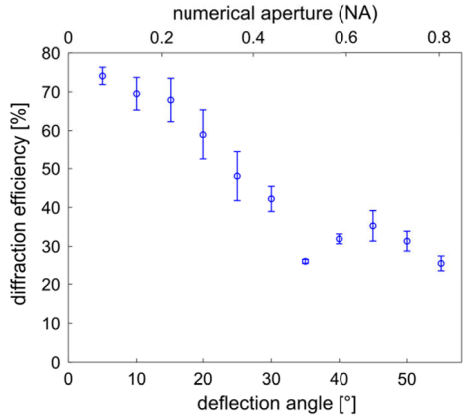

Fig. 2. Measured diffraction efficiencies of 3D printed linear gratings with varying deflection angle. All gratings were designed with a circular footprint and a diameter of 200 µm. Each grating type was printed three times and then measured individually. Error bars are indicating the standard deviation between single measurements of the three different prints.

In order to experimentally demonstrate the aberration correction capability of multiple elements, designs with a high numerical aperture (NA) of 0.8 were developed. Figures 3(A), 3(B), and 3(C) depict the design results of a singlet lens, a doublet, and a triplet lens with focal lengths of 67.5 µm, 78,8 µm, and 83,8 µm, respectively. Compared to singlet and triplet, the doublet lens was chosen smaller in terms of diameter and height while the designed NA is the same for all three devices. The individual aperture diameter (singlet: 180 µm, doublet: 140 µm, triplet: 180 µm) was selected to ensure a maximum space-bandwidth product and, if necessary, to trade image size and light throughput for less aberrations. The corresponding optimized phase profiles (Figs. 3(B), 3(F), and 3(J)) show significant deviations from conventional parabolic profiles.

In Figs 3(C), 3(G), and 3(K), corresponding CAD geometries are compared. The 3D printed results (Figs. 3(D), 3(H), and 3(L)) show good agreement with the design. Since the quality of the surface relief is crucial for efficiency and imaging performance, measurements with an atomic force microscope were performed. Figures 3(M) and 3(N) display the results of this measurement and its location on the sample. The cross section (Fig. 3(O)) indicates a smooth surface without notable staircasing effects. The small width of the steep slope Fresnel zone region of ~0.5 µm is on par if not better compared to most state-of-the-art direct writing approaches such as grey tone direct laser writing or electron beam lithography [37].

Optics EXPRESS

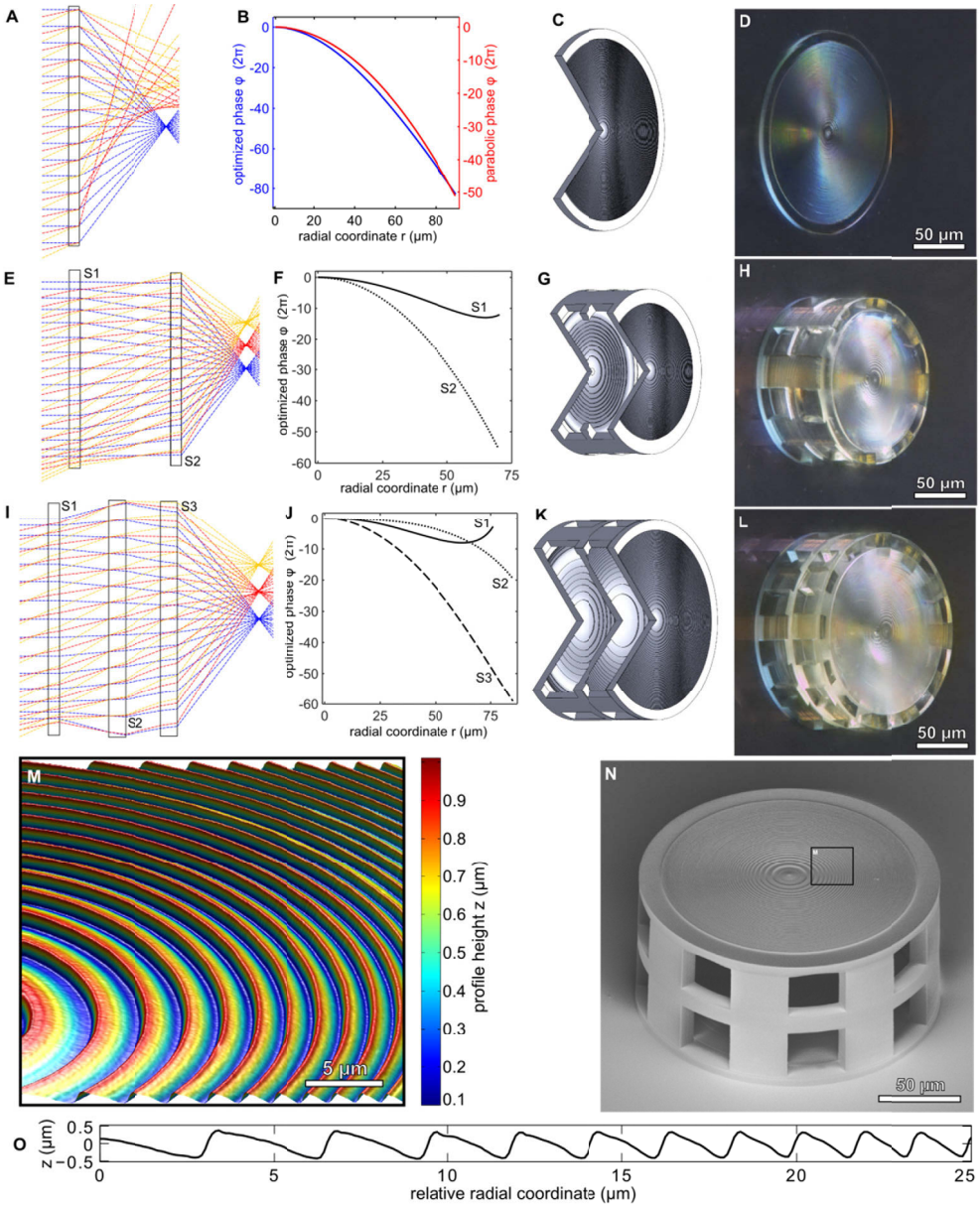

Fig. 3. Optical design, CAD design and fabrication results. (A) Single diffractive lens with a designed NA of 0.8. (B) Optimized phase function of the diffractive singlet in comparison with a conventional parabolic profile. (C) CAD design of the singlet lens. (D) Microscope image of the fabricated singlet lens. (E,F,G,H) Optical design, phase functions, CAD model and microscope image of the fabricated doublet lens with two diffractive surfaces S1 and S2. (I,J,K,L). Optical design, phase functions, CAD model and microscope image of the triplet lens with three diffractive surfaces. (M) Atomic force microscope measurement of the surface of the diffractive doublet lens. (N) SEM micrograph of the same lens. (O) Radial cross section of the phase relief, measured with the AFM.

Optics EXPRESS

Figure 4 depicts the imaging performance of a custom United States Air Force (1951 USAF chart) resolution-target for two different wavelength bands. In Figs. 4(A)–4(C) we compare the images recorded by singlet, doublet, and triplet lenses for green light with $\lambda = 550 \pm 20$ nm. Field dependent aberrations like coma and astigmatism decrease visibly with the number of stacked elements, and the image becomes sharper in its outer regions. At the same time, the higher number of interfaces appears to increase stray light and lowers the overall contrast. Similarly, the stacking of several DOEs reduces the overall diffraction efficiency. Compared to the singlet, the triplet has four additional polymer-to-air interfaces, each contributing with dielectric reflections and diffraction into unwanted orders. This effect will be reduced in the future using anti-reflection coatings and further optimization of diffraction efficiency. All images exhibit a barrel distortion which was not eliminated completely in the optical design due to a trade-off with other aberrations. In diffractive lenses, unwanted diffraction orders usually manifest in ghost images which are absent here. For the use as a camera, the white light performance is of high importance. Figures 4(D)–4(F) show the imaging results for illumination with a halogen bulb. Even though the system has not been optimized for color, e.g., by working in higher diffraction orders or using the methods from [38], the imaging performance is still good enough to resolve many of the features. This can be explained by the small overall size of the lenses as chromatic aberration scales with the lens size. The magnitude of color aberration, noticeable on the visible color seams, is on a level where its reduction becomes possible using digital methods [39].

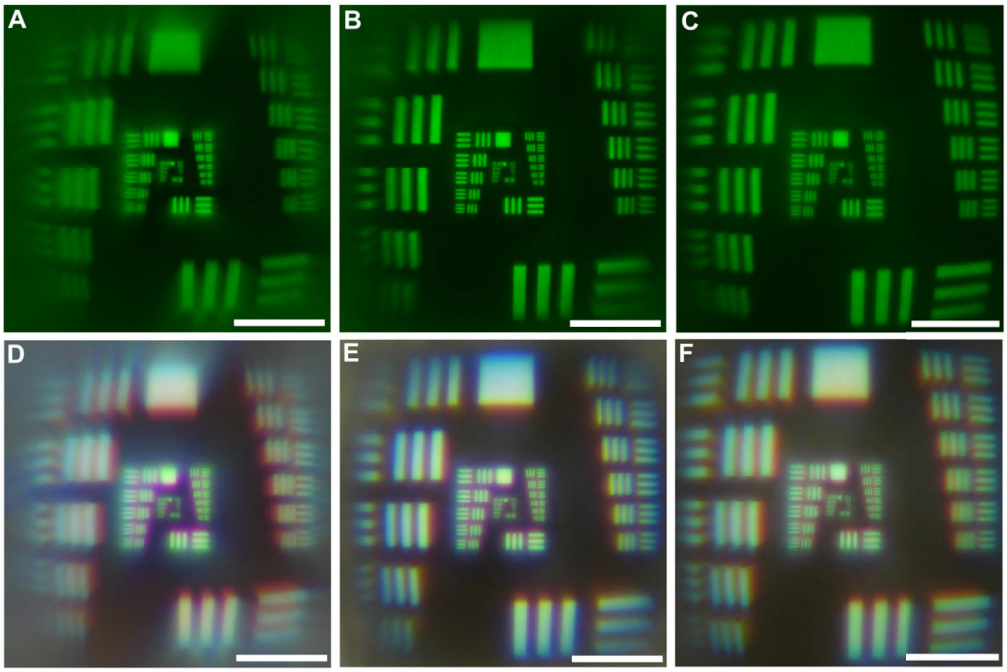

Fig. 4. Imaging performance of diffractive singlet, doublet, and triplet DOEs (scale bars: 25 µm). (A, B, C) Imaging through singlet, doublet, and triplet lenses with $\lambda = 550 \pm 20$ nm. Image recorded as depicted in Fig. 4(C). (D, E, F) Imaging through singlet, doublet, and triplet lenses using white light illumination (halogen bulb).

In order to evaluate the optical performance quantitatively, the normalized sagittal modulation MTF of the diffractive doublet lens is compared in Fig. 5(A) for angles of incidence of 0°, 15°, and 30° at $\lambda = 550 \pm 20$ nm. The results show that high contrasts can be obtained over the whole field of view and more than 1000 line pairs per mm at the Rayleigh resolution limit are resolvable.

Optics EXPRESS

It should be noted that the significant amount of stray light present in the images is not included in the MTF curves because of their normalization. When a knife edge is placed at the center of the field of view Michelson contrasts of approximately 71% (singlet), 95% (doublet), and 74% (triplet) between the bright and the dark regions can be measured using the NA 0.55 objective lens.

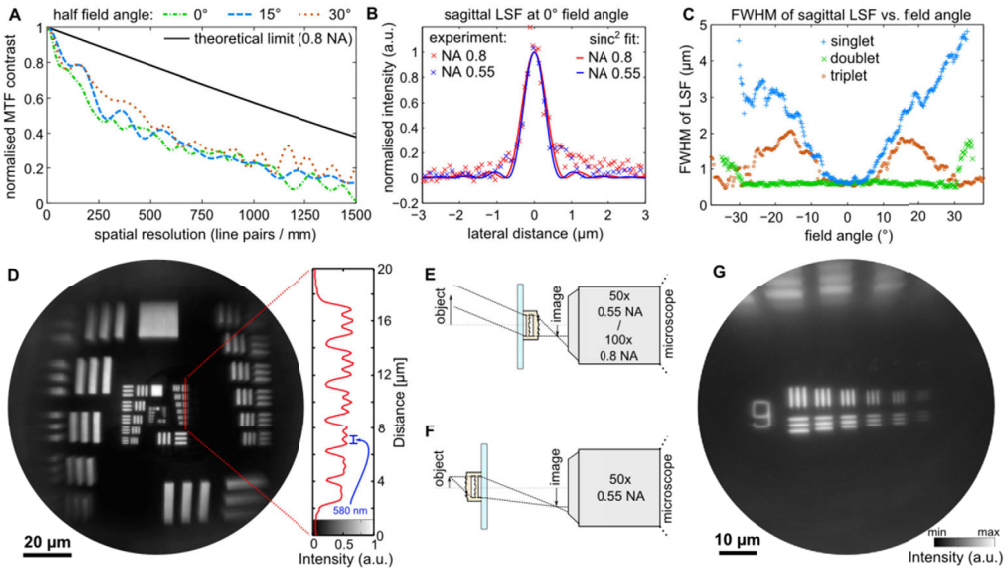

Fig. 5. Results of MTF and LSF measurement as well as direct imaging. (A) Sagittal MTF curves of a diffractive doublet lens for three different field angles of 0°, 15°, and 30° at $\lambda = 550 \pm 20$ nm. All curves are normalized to their maximum value. (B) Sagittal line-spread function (LSF) of a diffractive doublet lens at 0° field angle and $\lambda = 550 \pm 20$ nm measured with two different microscope objectives (0.55 NA and 0.8 NA). (C) Sagittal line-spread function (LSF) at $\lambda = 550 \pm 20$ nm as a function of field angle for singlet doublet and triplet. (D) Image taken with the doublet and $\lambda = 550 \pm 20$ nm with corresponding intensity cross section. A feature size of <580 nm can be resolved with a contrast of approximately 10%. (E) Measurement setup in the "camera" configuration. The object is placed beyond the hyperfocal distance and the image is formed at the focal plane of the diffractive lens. This image is then re-imaged onto a CMOS sensor by a microscope system. (F) Measurement setup for direct imaging. The object is placed very close to the focal plane of the 3D printed lens. (G) Result of direct imaging as displayed in (F). Element 6 of Group 9 of the USAF-Target is clearly resolved. This corresponds to a spatial frequency of 912.3 line pairs per mm.

Measurements of the sagittal line-spread function (LSF) reveal a full width at half maximum (FWHM) value of ~650 nm in the center of the field of view for the doublet lens (Fig. 5(B)). This corresponds to an effective NA of ~0.43 which is lower than the design value of 0.8. Figure 5(B) further confirms that the LSF does not change when observed with microscope objectives of increasing NA (0.55 and 0.8). This shows that the measured performance is not limited by the microscope lens with 0.55 NA which was mainly used for reasons of practicality.

When plotted versus the field angle (Fig. 5(C)), the FWHM values of the sagittal line-spread function reveal the superior performance of the doublet lens compared to singlet and triplet confirming the results from Fig. 4. While a singlet lens cannot reach aplanatic performance, the triplet, although superior in the design to the doublet, suffers from its increased number of interfaces and higher sensitivity on fabrication tolerances. The doublet lens shows a FWHM of

Optics EXPRESS

the sagittal line-spread function of 500-700 nm over a full field angle of 60°. To further assess the maximum resolution, images of the doublet lens were investigated in terms of contrast. The results are displayed in Fig. 5(D) for the configuration as displayed in Fig. 5(E), and in Fig. 5(G) for the configuration related to Fig. 5(F). The profile plot in Fig. 5(D) reveals a directly measured resolution of 580 nm at approximately 10% of remaining image contrast. The direct imaging in Fig. 5(G) proves that Group 9.6 of the USAF-target can still be resolved which corresponds to a resolution of 912.3 line pairs per mm.

4. Discussion

Our experiments demonstrate that the combination of multiple diffractive lenses, fabricated in one single step by femtosecond 3D printing, enables highly compact imaging systems for visible wavelengths. According to theory, one diffractive lens element allows perfect imaging only for one point, two surfaces permit a correction of the main first-order aberrations, and three surfaces help to further improve the performance at high numerical apertures or high field angles.

With sizes of below 200 µm in diameter and 100 µm in height, our lenses resolve line spacings of 580 nm at a wavelength of 550 nm and over a FWHM bandwidth of 40 nm. With two stacked planar lenses we could measure a FWHM of the sagittal line spread function of below 700 nm over a wide field of view of 60°. The corresponding imaging resolution of <800 nm according to the Rayleigh criterion is lower than the pixel pitch of today's image sensors. As expected, the performance deteriorates visibly when broadband illumination is used.

The method of femtosecond 3D printing is inherently alignment free and highly precise at the same time. Typical stitching-free write field diameters range from 200 µm to >1 mm depending on writing objective lens NA. One of its main drawbacks, hour-long fabrication times, is diminished because the lenses only require a small amount of material. This is due to the fact that diffraction happens only at the phase relief layers which are less than 1 µm in thickness. Currently, the writing time is about 15 minutes for a doublet lens but can be further reduced if the mounting disks are made thinner and the support structures are written with coarser line spacing. Compared to other designs investigated by the authors based on conventional lenses or curved diffractive aplanats, the flat diffractive lenses show superior optical performance.

To further improve the devices, it is important to realize absorbing apertures [40] and shells in order to decrease stray light. Also, antireflective coatings could help to reduce dielectric losses. The blazed diffractive structures could be optimized in order to increase diffraction efficiency, especially for high deflection angles, by using designs as presented in [41] or [42]. In principle, structures using total internal reflection could be integrated in order to achieve high angle diffraction efficiencies closer to what is possible with metasurfaces [43] or blazed binary gratings [44]. Accurate simulation algorithms are an important tool to improve the designs [45,46]. In principle, our technology allows a reduction of chromatic aberration if multiple diffraction orders are combined in one element and the lenses have shapes as described in [17] and [38].

Our approach opens the possibility for high resolution imaging on smallest size scales which is particularly interesting for applications in endoscopy, small surveillance camera vision, or security, as well as for smartphones, imaging sensors, and augmented/virtual reality displays. If used in reverse, the lenses could act as small scale microscope objective lenses towards diffraction-limited imaging quality. Moreover, thanks to their extremely low weight of less than 1 µg, 3D-printed lens stacks could also be interesting for space applications. As a prime example, the first interstellar missions based on laser propulsion as suggested from the Breakthrough Starshot initiative [46] would have to rely on ultra-lightweight optical components.

Optics EXPRESS

Funding

Bundesministerium für Bildung und Forschung (13N14097); Baden-Württemberg Stiftung (Opterial); European Research Council; Deutsche Forschungsgemeinschaft.

Acknowledgments

We thank Prof. Gregory I. Greisukh for his help with the literature research, Mario Hentschel for the fabrication of a high resolution USAF test target, Simon Ristok for support with fabrication and measurement and Dr. Liwei Fu for taking the SEM images.

References

1. C. Liberale, G. Cojoc, P. Candeloro, G. Das, F. Gentile, F. de Angelis, and E. Di Fabrizio, "Micro-Optics Fabrication on Top of Optical Fibers Using Two-Photon Lithography," IEEE Photonics Technol. Lett. **22**(7), 474–476 (2010).
2. H. E. Williams, D. J. Freppon, S. M. Kuebler, R. C. Rumpf, and M. A. Melino, "Fabrication of three-dimensional micro-photonic structures on the tip of optical fibers using SU-8," Opt. Express **19**(23), 22910–22922 (2011).
3. T. Gissibl, S. Thiele, A. Herkommer, and H. Giessen, "Two-photon direct laser writing of ultracompact multi-lens objectives," Nat. Photonics **10**(8), 554–560 (2016).
4. T. Gissibl, S. Thiele, A. Herkommer, and H. Giessen, "Sub-micrometre accurate free-form optics by three-dimensional printing on single-mode fibres," Nat. Commun. **7**(1), 11763 (2016).
5. Q.-D. Chen, D. Wu, L.-G. Niu, J. Wang, X.-F. Lin, H. Xia, and H.-B. Sun, "Phase lenses and mirrors created by laser micronanofabrication via two-photon photopolymerization," Appl. Phys. Lett. **91**(17), 171105 (2007).
6. E. Brasselet, M. Malinauskas, A. Žukauskas, and S. Juodkazis, "Photopolymerized microscopic vortex beam generators. Precise delivery of optical orbital angular momentum," Appl. Phys. Lett. **97**(21), 211108 (2010).
7. V. Osipov, L. L. Doskolovich, E. A. Bezus, W. Cheng, A. Gaidukeviciute, and B. Chichkov, "Fabrication of three-focal diffractive lenses by two-photon polymerization technique," Appl. Phys. A **107**(3), 525–529 (2012).
8. T. Gissibl, M. Schmid, and H. Giessen, "Spatial beam intensity shaping using phase masks on single-mode optical fibers fabricated by femtosecond direct laser writing," Optica **3**(4), 448 (2016).
9. S. Lightman, R. Gvishi, G. Hurvitz, and A. Arie, "Shaping of light beams by 3D direct laser writing on facets of nonlinear crystals," Opt. Lett. **40**(19), 4460–4463 (2015).
10. M. F. Schumann, S. Wiesendanger, J. C. Goldschmidt, B. Bläsi, K. Bittkau, U. W. Paetzold, A. Sprafke, R. B. Wehrspohn, C. Rockstuhl, and M. Wegener, "Cloaked contact grids on solar cells by coordinate transformations. Designs and prototypes," Optica **2**(10), 850 (2015).
11. T. Ergin, N. Stenger, P. Brenner, J. B. Pendry, and M. Wegener, "Three-dimensional invisibility cloak at optical wavelengths," Science **328**(5976), 337–339 (2010).
12. A. J. Fresnel, "Calcul de l'intensité de la lumière au centre de l'ombre d'un ecran et d'une ouverture circulaires eclairés par un point radieux," in *Œuvres Complètes d'Augustin Fresnel*, Henri de Senarmont, ed. (1866), pp. 365–372.
13. K. Miyamoto, "The Phase Fresnel Lens," J. Opt. Soc. Am. **51**(1), 17–20 (1961).
14. J. A. Jordan, P. M. Hirsch, L. B. Lesem, and D. L. van Rooy, "Kinoform lenses," Appl. Opt. **9**(8), 1883–1887 (1970).
15. R. M. Henkelman and M. J. Bronskill, "Imaging extended objects with a Fresnel-zone-plate aperture," J. Opt. Soc. Am. **64**(2), 134–137 (1974).
16. J. N. Mait, A. Scherer, O. Dial, D. W. Prather, and X. Gao, "Diffractive lens fabricated with binary features less than 60 nm," Opt. Lett. **25**(6), 381–383 (2000).
17. M. Rossi, R. E. Kunz, and H. P. Herzig, "Refractive and diffractive properties of planar micro-optical elements," Appl. Opt. **34**(26), 5996–6007 (1995).
18. M. T. Gale, M. Rossi, H. Schütz, P. Ehbets, H. P. Herzig, and D. Prongué, "Continuous-relief diffractive optical elements for two-dimensional array generation," Appl. Opt. **32**(14), 2526–2533 (1993).
19. M. A. Kats, P. Genevet, N. Yu, R. Blanchard, Z. Gaburro, and F. Capasso, "Aberration-free ultrathin flat lenses and axicons at telecom wavelengths based on plasmonic metasurfaces," Nano Lett. **12**(9), 4932–4936 (2012).
20. D. Lin, P. Fan, E. Hasman, and M. L. Brongersma, "Dielectric gradient metasurface optical elements," Science **345**(6194), 298–302 (2014).
21. A. Arbabi, Y. Horie, M. Bagheri, and A. Faraon, "Dielectric metasurfaces for complete control of phase and polarization with subwavelength spatial resolution and high transmission," Nat. Nanotechnol. **10**(11), 937–943 (2015).
22. M. Khorasaninejad, W. T. Chen, R. C. Devlin, J. Oh, A. Y. Zhu, and F. Capasso, "Metalenses at visible wavelengths. Diffraction-limited focusing and subwavelength resolution imaging," Science **352**(6290), 1190–1194 (2016).
23. S. Wang, P. C. Wu, V.-C. Su, Y.-C. Lai, M.-K. Chen, H. Y. Kuo, B. H. Chen, Y. H. Chen, T.-T. Huang, J.-H. Wang, R.-M. Lin, C.-H. Kuan, T. Li, Z. Wang, S. Zhu, and D. P. Tsai, "A broadband achromatic metalens in the visible," Nat. Nanotechnol. **13**(3), 227–232 (2018).
24. W. T. Chen, A. Y. Zhu, V. Sanjeev, M. Khorasaninejad, Z. Shi, E. Lee, and F. Capasso, "A broadband achromatic metalens for focusing and imaging in the visible," Nat. Nanotechnol. **13**(3), 220–226 (2018).

Optics EXPRESS

25. D. Faklis and G. M. Morris, "Broadband Imaging With Holographic Lenses," Opt. Eng. **28**(6), 286592 (1989).
26. F. Aieta, P. Genevet, M. Kats, and F. Capasso, "Aberrations of flat lenses and aplanatic metasurfaces," Opt. Express **21**(25), 31530–31539 (2013).
27. W. T. Welford, "Aplanatic hologram lenses on spherical surfaces," Opt. Commun. **9**(3), 268–269 (1973).
28. N. Bokor and N. Davidson, "Aberration-free imaging with an aplanatic curved diffractive element," Appl. Opt. **40**(32), 5825–5829 (2001).
29. G. I. Grejsuch, S. T. Bobrov, and S. A. Stepanov, *Optics of diffractive and gradient-index elements and systems* (SPIE Optical Engineering Press, 1997).
30. D. A. Buralli and G. M. Morris, "Design of a wide field diffractive landscape lens," Appl. Opt. **28**(18), 3950–3959 (1989).
31. A. Arbabi, E. Arbabi, S. M. Kamali, Y. Horie, S. Han, and A. Faraon, "Miniature optical planar camera based on a wide-angle metasurface doublet corrected for monochromatic aberrations," Nat. Commun. **7**(1), 13682 (2016).
32. B. Groever, W. T. Chen, and F. Capasso, "Meta-Lens Doublet in the Visible Region," Nano Lett. **17**(8), 4902–4907 (2017).
33. T. Gissibl, S. Wagner, J. Sykora, M. Schmid, and H. Giessen, "Refractive index measurements of photo-resists for three-dimensional direct laser writing," Opt. Mater. Express **7**(7), 2293 (2017).
34. P. Lalanne, S. Astilean, P. Chavel, E. Cambril, and H. Launois, "Design and fabrication of blazed binary diffractive elements with sampling periods smaller than the structural cutoff," J. Opt. Soc. Am. A **16**(5), 1143–1156 (1999).
35. V. P. Korolkov, R. K. Nasyrov, and R. V. Shimansky, "Zone-boundary optimization for direct laser writing of continuous-relief diffractive optical elements," Appl. Opt. **45**(1), 53–62 (2006).
36. U. Levy, D. Mendlovic, and E. Marom, "Efficiency analysis of diffractive lenses," J. Opt. Soc. Am. A **18**(1), 86–93 (2001).
37. E.-B. Kley, "Continuous profile writing by electron and optical lithography," Microelectron. Eng. **34**(3-4), 261–298 (1997).
38. D. Faklis and G. M. Morris, "Spectral properties of multiorder diffractive lenses," Appl. Opt. **34**(14), 2462–2468 (1995).
39. S.-W. Chung, B.-K. Kim, and W.-J. Song, "Detecting and eliminating chromatic aberration in digital images," *ICIP'09 Proceedings of the 16th IEEE international conference on Image processing*, 3861–3864 (2009).
40. A. Toulouse, S. Thiele, H. Giessen, and A. M. Herkommer, "Alignment-free integration of apertures and nontransparent hulls into 3D-printed micro-optics," Opt. Lett. **43**(21), 5283–5286 (2018).
41. E. Noponen, J. Turunen, and A. Vasara, "Electromagnetic theory and design of diffractive-lens arrays," J. Opt. Soc. Am. A **10**(3), 434 (1993).
42. K. Blomstedt, E. Noponen, and J. Turunen, "Surface-profile optimization of diffractive 1:1 imaging lenses," J. Opt. Soc. Am. A **18**(3), 521 (2001).
43. D. Lin, M. Melli, E. Poliakov, P. St. Hilaire, S. Dhuey, C. Peroz, S. Cabrini, M. Brongersma, and M. Klug, "Optical metasurfaces for high angle steering at visible wavelengths," Sci. Rep. **7**(1), 2286 (2017).
44. U. Levy, E. Marom, and D. Mendlovic, "Thin element approximation for the analysis of blazed gratings. Simplified model and validity limits," Opt. Commun. **229**(1-6), 11–21 (2004).
45. S. Schmidt, S. Thiele, A. Herkommer, A. Tünnermann, and H. Gross, "Rotationally symmetric formulation of the wave propagation method-application to the straylight analysis of diffractive lenses," Opt. Lett. **42**(8), 1612–1615 (2017).
46. G. Popkin, "What it would take to reach the stars," Nature **542**(7639), 20–22 (2017).